Supporting Information for

Penguin feather-inspired flexible aerogel composite films featuring ultra-low thermal conductivity and dielectric constant

Rui Yang[1], Kexing Yu[1], Xiang Yu[1,*], Wenqi Zhang[1], Kaixuan Sun[1], Fangcheng Lv[1], Yunpeng Liu[1], Sidi Fan[1,*]

[1]*State Key Laboratory of Alternate Electrical Power System with Renewable Energy Sources, School of Electrical and Electronic Engineering, North China Electric Power University, Beijing 102206, People's Republic of China*

*Corresponding authors.

E-mail: sidifan@ncepu.edu.cn (S.F); xiangyu@ncepu.edu.cn (X.Y)

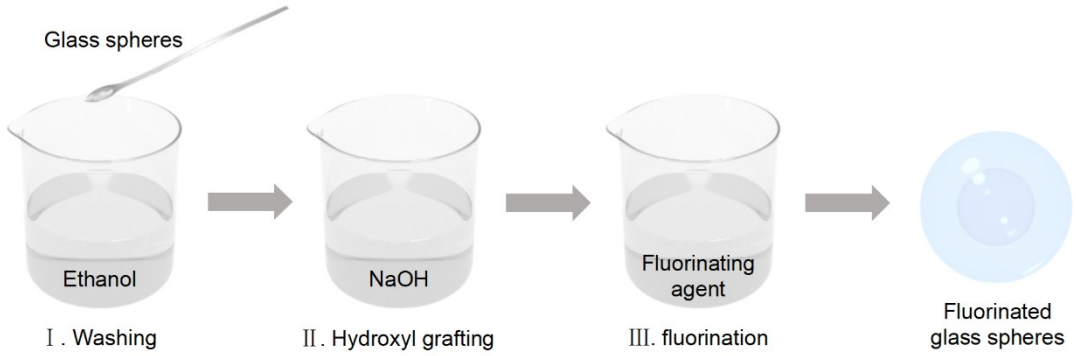

Figure S1. The whole preparation process of fluorinated glass spheres.

Note 1. Mechanism of fluorination treatment

According to the characterization of silane coupling agents, PFDTES is spontaneously hydrolyzed in aqueous solvent to generate hydroxyl-rich silanol.[1] When the silanol and hydroxylated glass spheres are dispersed in solution, the dehydration reaction will occur at a steady rate at room temperature. The fluorinating groups will be grafted onto the surface of the glass spheres by covalent bonding.[2-3] Dehydration reactions also occur between the silanol on the surface of glass spheres, consuming the excessive hydroxyl groups.

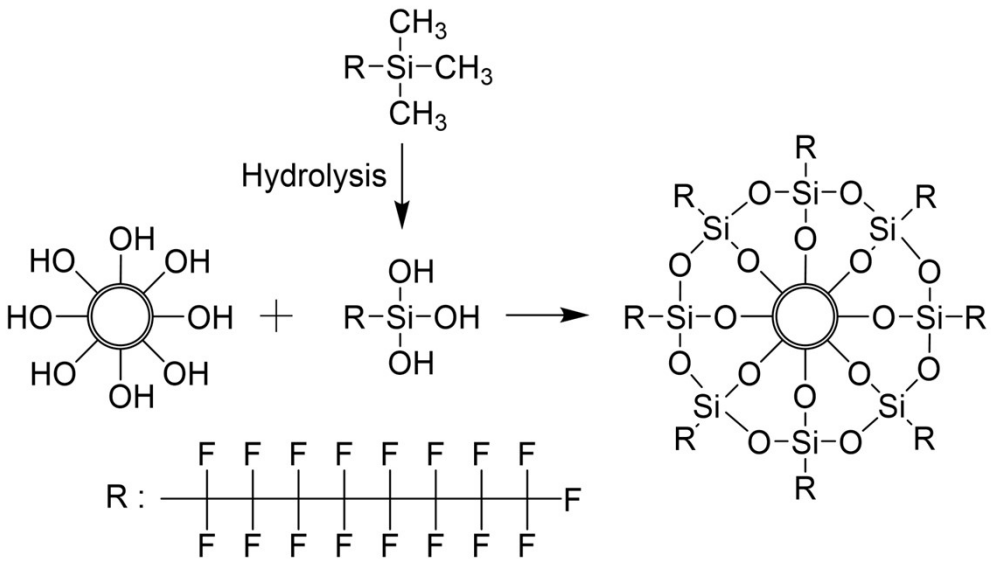

Figure S2. Reaction process of fluorination.

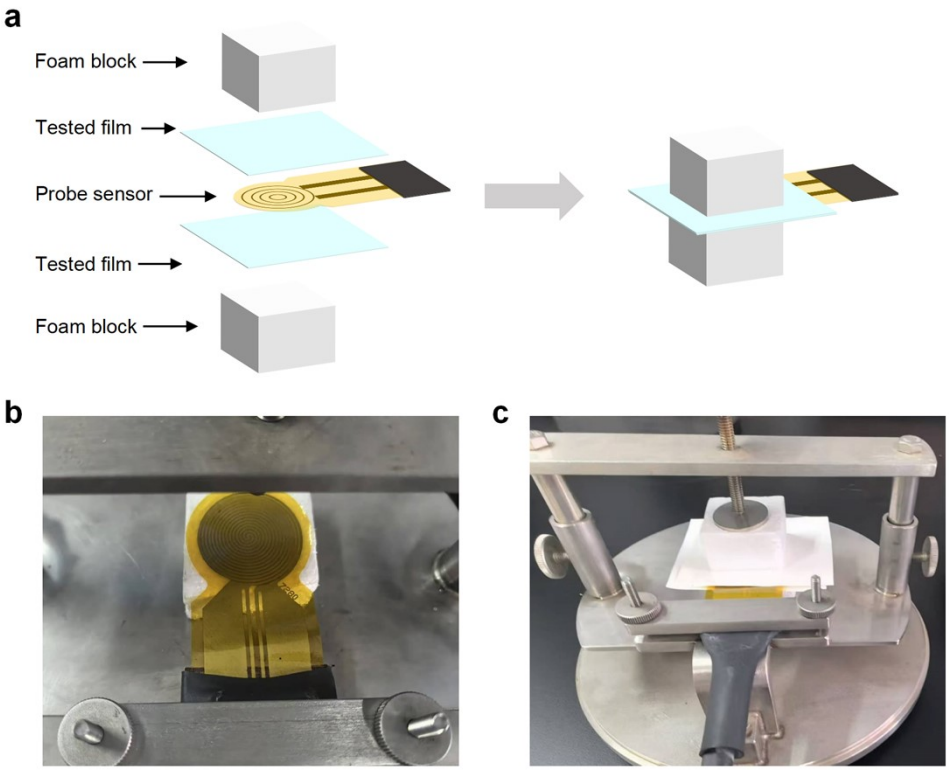

Figure S3. (a) Schematic illustrating the cross-section of the Hot Disk Test System. (b) The probe sensor of #7280 Kapton. (c) The Hot Disk Test System.

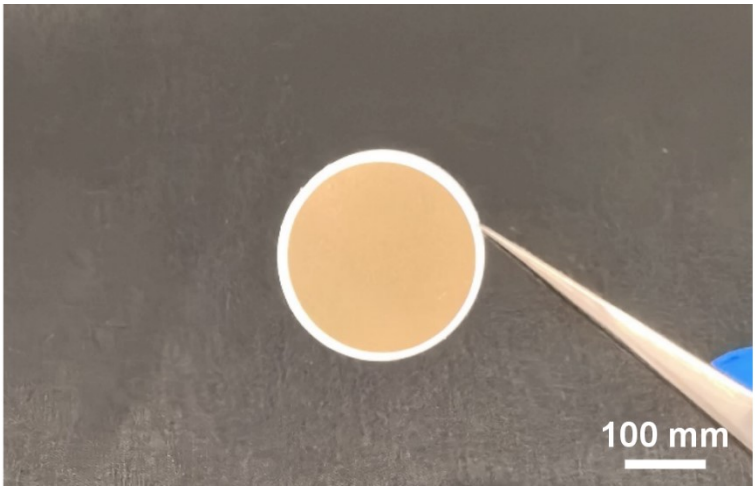

Figure S4. The gold electrode for dielectric testing.

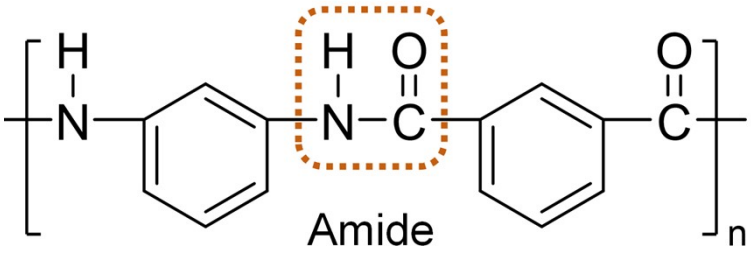

Figure S5. Chemical structure of PMIA.

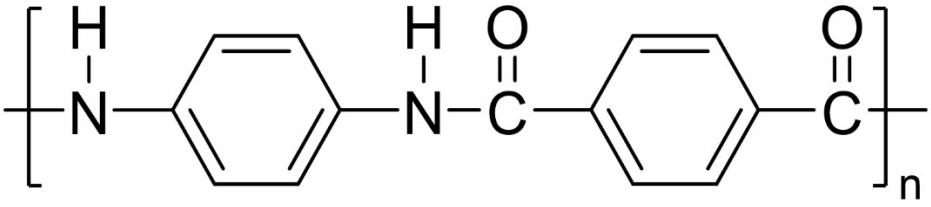

Figure S6. Chemical structure of PPTA.

Note 2. Density and thermal conductivity of PMIA based on DFT calculations

DFT calculations of PMIA molecules using *Materials Studio* (MS), the construction of the composite models, and the parameter settings are detailed as follows:

The PMIA model is manually constructed according to the molecular structure as shown in Figure S7a. The black balls in the diagram represent carbon atoms, the red balls represent O atoms, the blue balls represent N atoms, and the white balls represent H atoms. Subsequently, the hydrogen atoms on the carbon and nitrogen atoms at both ends of PMIA are set as the head and tail atoms, respectively, and they are constructed into a PMIA molecular chain with a degree of polymerization of 10 as shown in Figure S7b. Adding 15 PMIA chains to the PMIA cell as shown in Figure S7c, the force field and charge distribution are carried out through the *Amorphous Cell* module, and the geometry optimization is performed to minimize the energy.

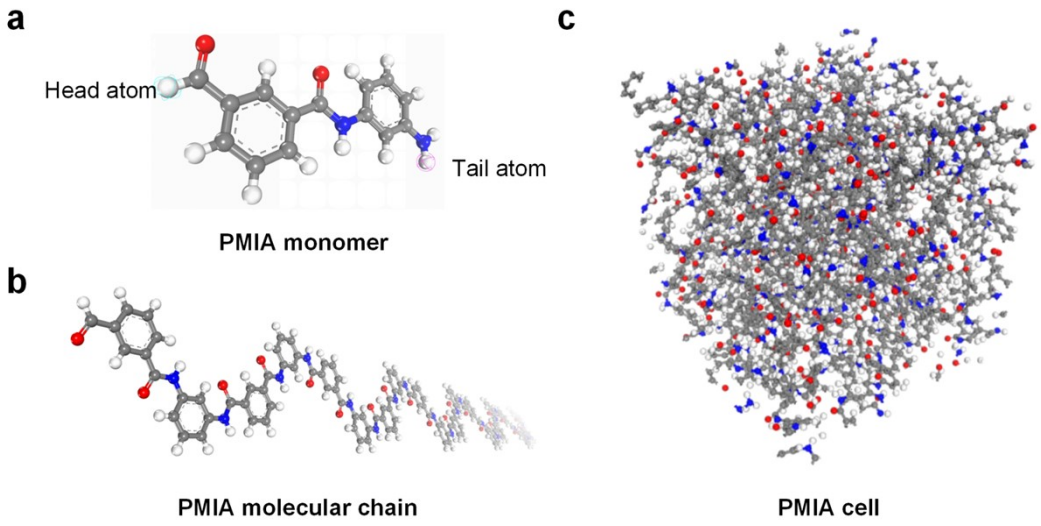

Figure S7. (a) PMIA monomer is constructed in DFT calculation. (b) PMIA molecular chain is constructed in DFT calculation. (c) PMIA cell is constructed in DFT calculation.

The initial models constructed above were in an unstable state and were first geometrically optimized to bring them to a reasonable conformation.[4] After that, to make the model closer to the actual material and to release the unreasonable internal stresses, the model was annealed for 25 cycles from 300 K to 700 K with the annealing time set to 500 ps, and then the NVT and NPT systems were selected to relax for 500 ps each at a temperature of 300 K and a pressure of 0.1 MPa, and then continued to be optimized so that their densities reached a stable value, i.e., the relaxation

equilibrium. As shown in Figure S8, the average value of density 1.258 g/cm^3 for the last 100 ps of the equilibrium process of PMIA system was taken as the simulated value. Finally, the model was ramped up from 300 K to 700 K in steps of 50 K intervals, and the models at each temperature gradient were subjected to 500 ps NVT and NPT relaxation, respectively, to finally obtain stable models at each temperature between 300 K and 700 K for subsequent thermodynamic property analysis. The above calculations were carried out under the *COMPASS III* force field, and the temperature and pressure were controlled by the Andersen and Berendsen method, and the van der Waals and electrostatic forces were controlled by the Atom-Based and Ewald methods.

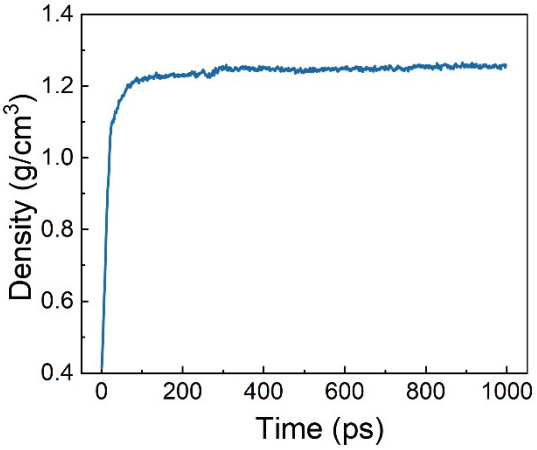

Figure S8. Density calculation for PMIA.

For the calculation of thermal conductivity, the local heat bath method is used to establish the temperature gradient.[5] Firstly, energy minimization calculations are performed for the system, followed by 500 ps relaxation under the NPT system for system equilibrium, and then 500 ps kinetic calculations under the NVT system for analyzing the temperature and energy flow. The Non-Equilibrium Molecular Dynamics (NEMD) method uniformly cuts the model into several layers (in this paper, a total of 100) along a certain direction (the X direction is chosen for the present paper), and the layer located on the leftmost side of the system is called the "heat source", the rightmost layer is called "heat sink", and the temperature control method of Langevin is used in the two regions to keep them at the preset temperatures (preset value of the heat source layer is 350 K, and the preset value of the heat sink layer is 250 K. The NEMD model is illustrated in Figure S9. The cold particles in the heat source layer and the hot particles in the heat sink layer are continuously exchanging

energy, and eventually a stable temperature gradient is gradually formed in the system, heat flux of PMIA cell is shown in Figure S10.

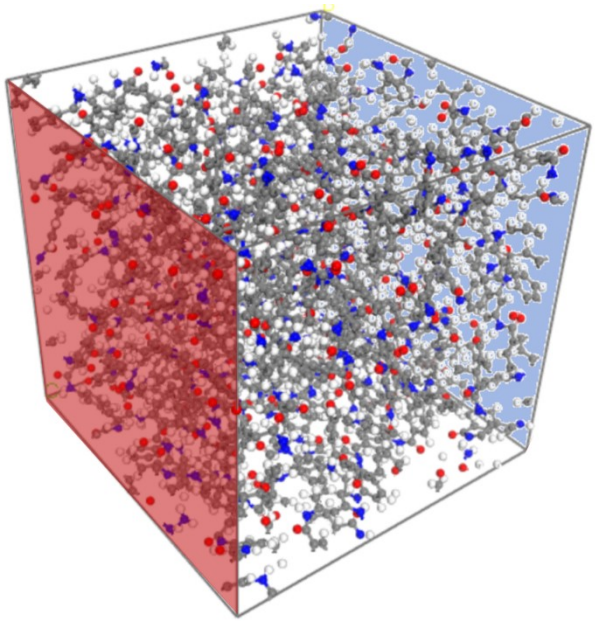

Figure S9. Schematic of the NEMD model.

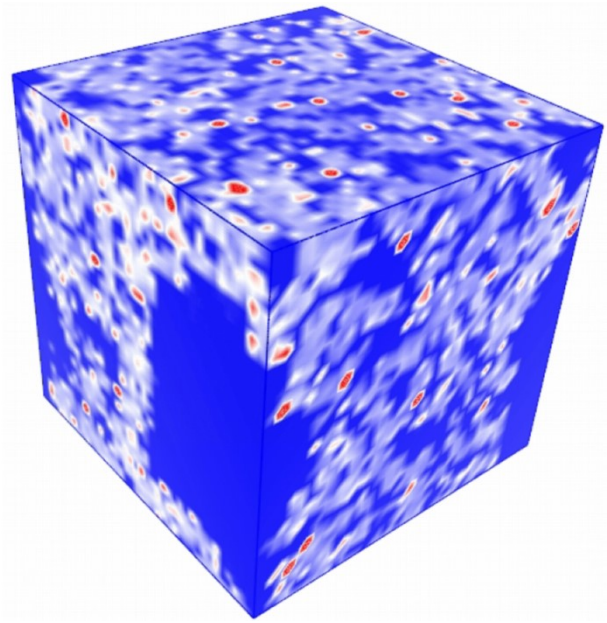

Figure S10. Heat flux of PMIA cell.

The thermal conductivity of the system is obtained by Fourier heat transfer[6]:

$$\kappa = -\frac{J}{A\Delta T} \tag{S1}$$

$$J = \frac{\partial M}{\partial t} \tag{S2}$$

$$\nabla T = \frac{\partial T}{\partial x} \tag{S3}$$

where J is the heat flow; A is the heat transfer area; T is the temperature; ∇T is the temperature gradient; M is the average of the absolute values of the inflow energy from the heat source and the heat sink; t is the simulation time; and x is the direction of heat transfer.

Note 3. Preparation process of the dense and compact PMIA film

To prepare the PMIA film with a dense and compact structure, the conventional solution casting method is adopted. Different from the sol-gel method, after casting the sol film, it is directly placed in a drying oven at 80°C for 24 h to remove the solvent, without undergoing the gelation treatment. After the hot-pressing treatment, a condensed PMIA film can be obtained. As shown in Figure S11, the film has a transparent appearance, with the SEM image indicating its condensed structure and a typical thickness of ~10 μm.

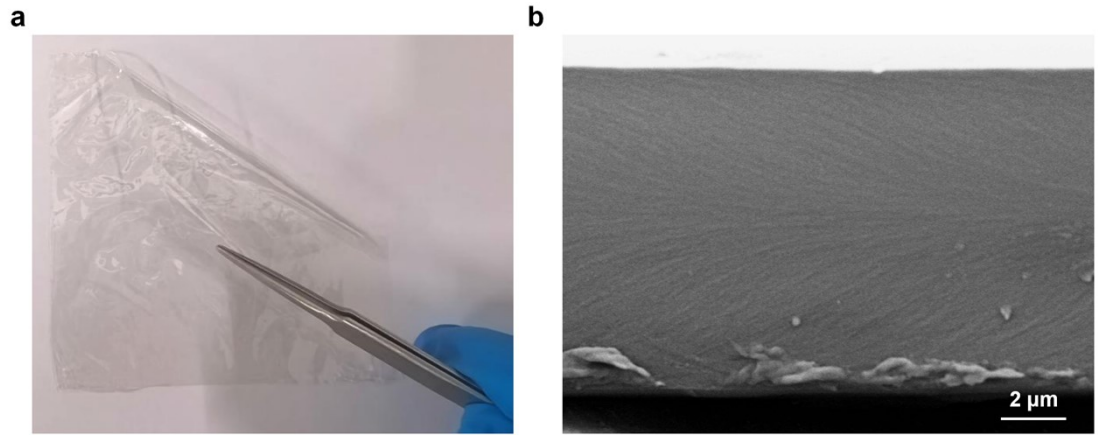

Figure S11. (a) The meta-aramid film prepared by the conventional solution casting method. (b) Cross-sectional morphology illustrating the condensed structure.

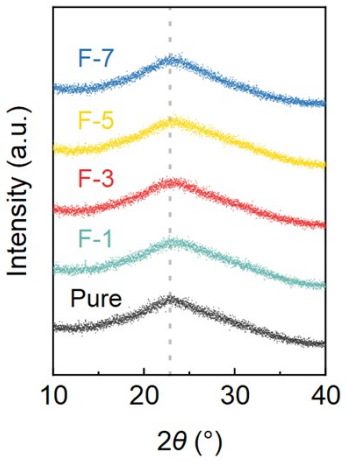

Figure S12. XRD patterns for various aerogel films.

Table S1. Thermal conductivity testing results of various films

Films	Thermal conductivity (mW/m·K)			Average	Standard deviation
	1	2	3		
Pure	31.9	32.6	32.5	32.3	0.379
OH-1	29.7	29.3	29.4	29.5	0.208
OH-3	25.5	24.8	25.1	25.1	0.351
OH-5	28.3	28.0	27.8	28.0	0.252
OH-7	29.2	28.9	30.0	29.4	0.569
F-1	24.8	25.2	25.0	25.0	0.200
F-3	21.8	21.8	21.1	21.6	0.404
F-5	23.3	23.5	23.7	23.5	0.200
F-7	26.4	26.3	25.8	26.2	0.321

Table S2. Thermal conductivity of representative polymer-based aerogel films.

Materials	Structures	Preparation methods	Thermal conductivity (mW/m·K)	References
Kevlar nanofiber aerogel (KNA)/phase-change materials (PCM)	Nanofibrous KNA film encapsulated by PCM	Freeze-drying	36.0	28
Ultrahigh molecular weight polyethylene (UHMW-PE)	Micro-macro hybrid porous structure	Thermal induced phase separation (TIPS) and particle leaching (PL)	34.0	29
Poly(dimethylsiloxane) (PDMS)/polyethylene (PE)	PDMS film laminated with PE nanoflake aerogel	Freeze-drying and lamination	32.0	30
Aramid nanofiber (ANF)	Asymmetric structure of a dense skin layer and a high-porous nanofibrous body	Freeze-drying	31.0	22
Silica-alumina nanofibrous aerogels (SAFAs)	Porous structure by anisotropic fibers	Electrostatic spinning	30.0	31
Poly(vinylidenefluofide-co-hexafluoropropylene (P(VdF-HFP))/glass fibers (GF)	Composited aerogel structure	Freeze-drying	28.9	32
Polyethylene aerogel (PEA)	Highly porous structure (>0.9)	TIPS	28.0	33
Polyimide (PI)	3D interconnected	Sol-gel	27.5	21

	porous network			
MXene-CNF/CNF	Janus structure	Freeze-drying	25.0	34
Meta-aramid/fluorinated hollow glass spheres aerogel films	Micro-nano porous structure	Sol-gel and hot-pressing	21.6	This work

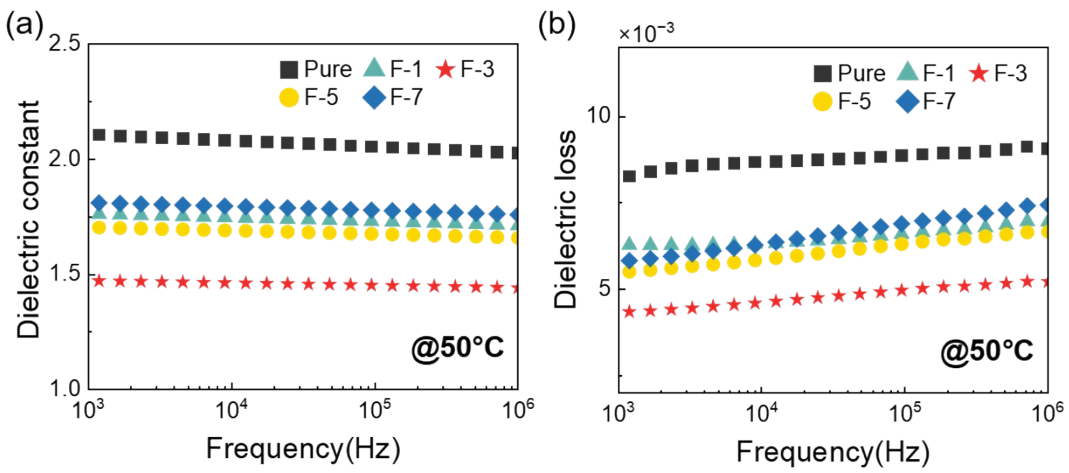

Figure S13. (a) Frequency-dependent dielectric constant and (b) dielectric loss of various aerogel films at 50°C.

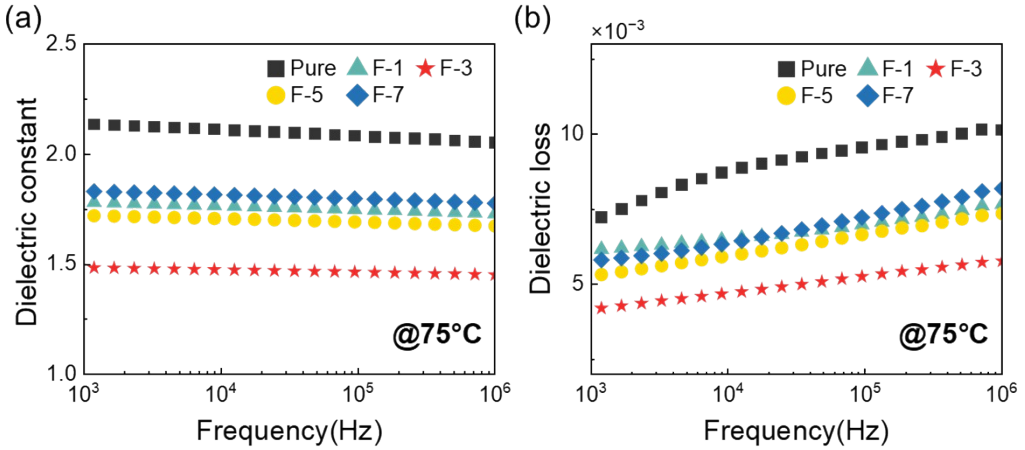

Figure S14. (a) Frequency-dependent dielectric constant and (b) dielectric loss of various aerogel films at 75°C.

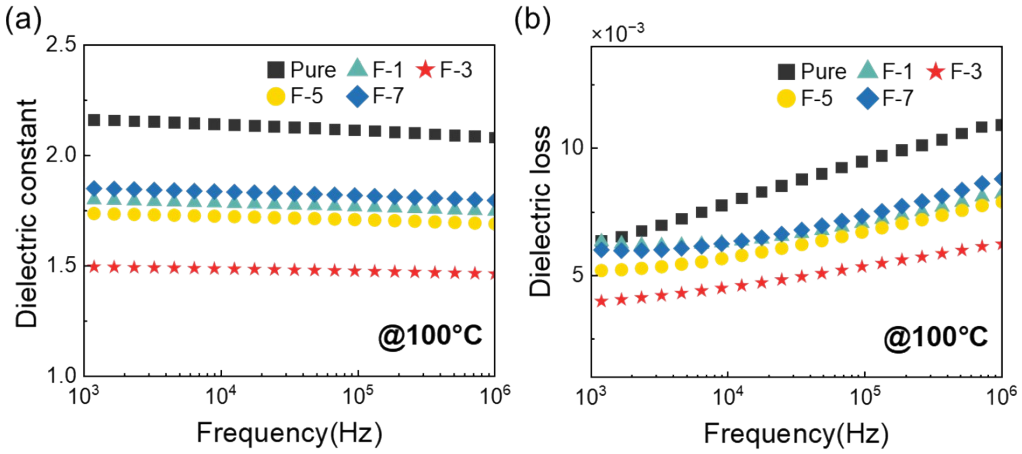

Figure S15. (a) Frequency-dependent dielectric constant and (b) dielectric loss of various aerogel films at 100°C.

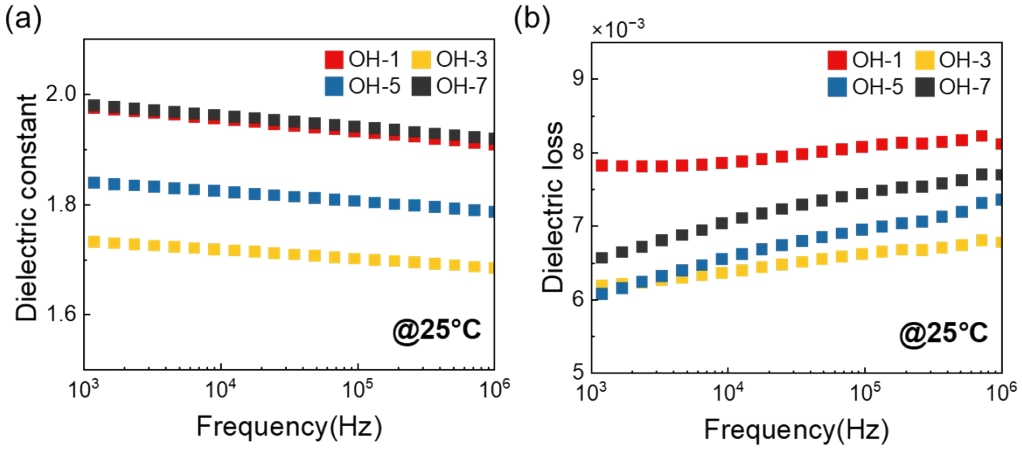

Figure S16. (a) Frequency-dependent dielectric constant and (b) dielectric loss of doping OH-glass sphere samples aerogel films at 25°C.

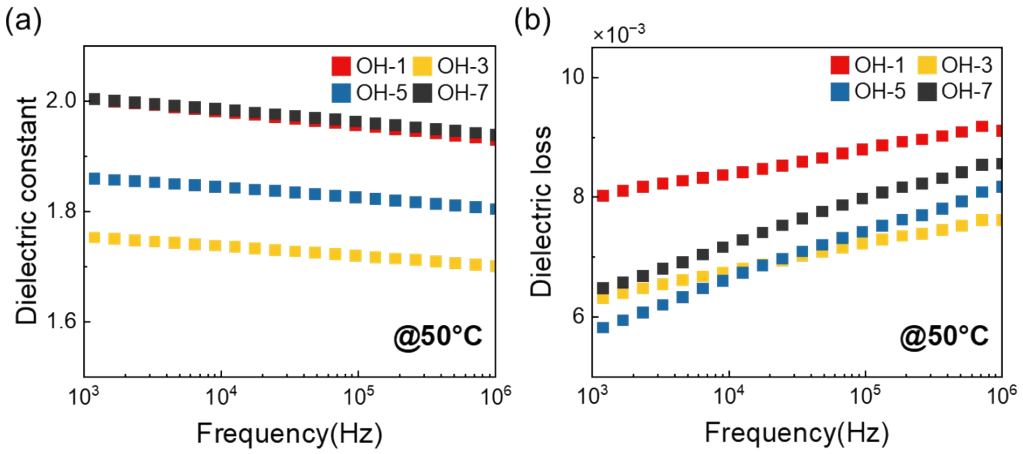

Figure S17. (a) Frequency-dependent dielectric constant and (b) dielectric loss of doping OH-glass sphere samples aerogel films at 50°C.

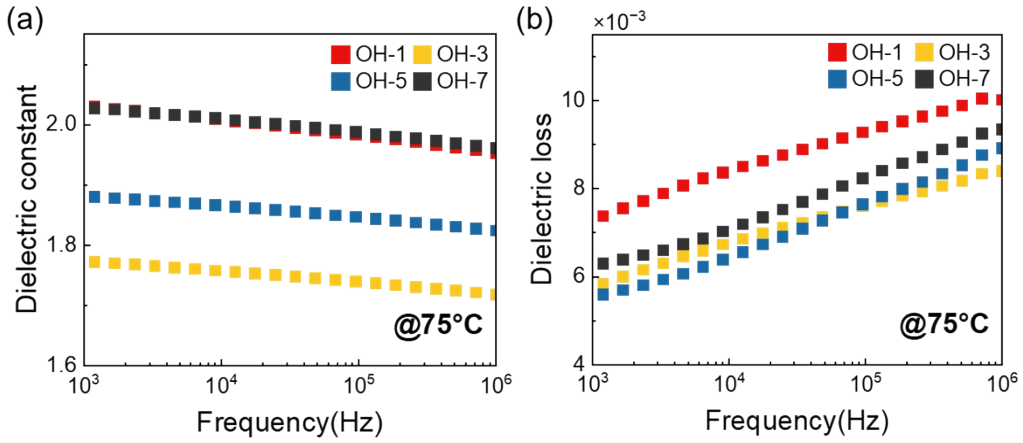

Figure S18. (a) Frequency-dependent dielectric constant and (b) dielectric loss of doping OH-glass sphere samples aerogel films at 75°C.

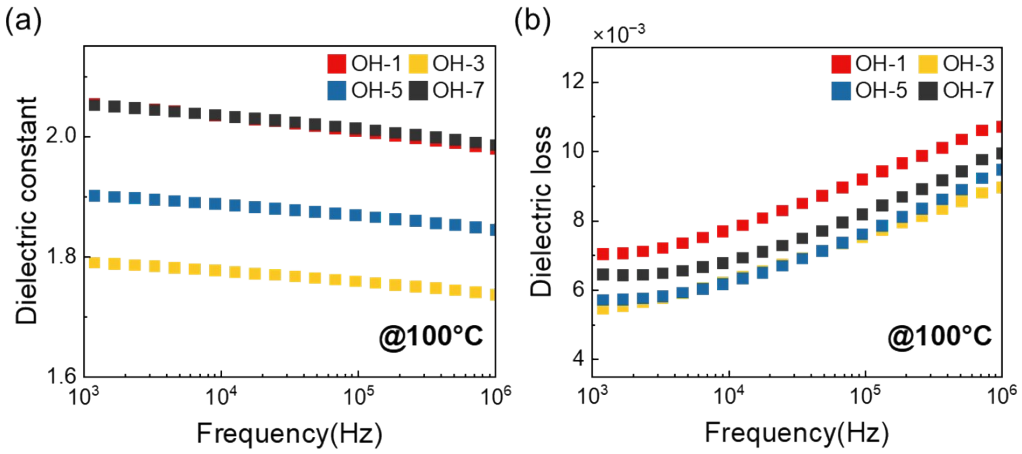

Figure S19. (a) Frequency-dependent dielectric constant and (b) dielectric loss of doping OH-glass sphere samples aerogel films at 100°C.

Note 4. Construction and parameter settings of FEM simulation

Based on the co-simulation using *MATLAB* and *COMSOL* Multiphysics, 2D FEM models of aerogel films are constructed. The coding flow diagram is shown in Figure S20.

A square with a side length of 40 μm was constructed as matrix, to which circles with a radius of 500 nm were added as pores. The addition of each new pore is judged by the traversal method to decide whether it intersects with the already existing pores. Once the judgment has been passed, the result is recorded in the geometric model and this pore volume is counted as part of the total pore content. If the total filler content exceeds the pore volume, a final resultant model with a specific loading volume is obtained. For the composite model, a ring with an outer diameter of 10 μm and a thickness of 250 nm was added as a glass sphere in the center of the square before adding pores.

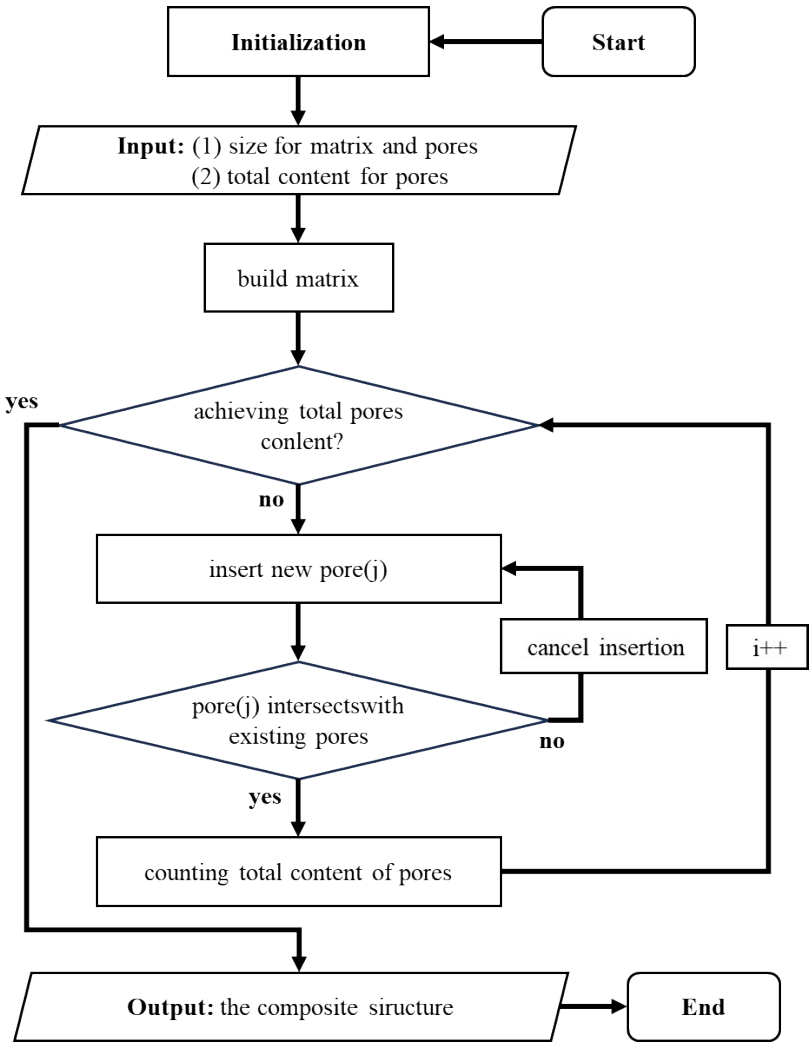

Figure S20. The code diagram of model construction.

In the FEM models, the electrostatic model built in *COMSOL* is used to calculate the distribution of the polarization, the solid heat transfer and fluid heat transfer model are used to calculate the distribution of the heat flow and the steady state properties of the composite system are analyzed by applying a voltage of 10 V on the top of the square, and a 50°C total difference in temperature between the top and bottom.

Table S3. The settings of materials parameters.

Materials	Density (g/cm^3)	Average molar mass (kg/mol)	Dielectric constant	Thermal conductivity (W/m·K)
PMIA	1.258	-	5.000	0.200
Air	-	0.029	1.000	0.025
Glass	2.200	-	1.560	1.400

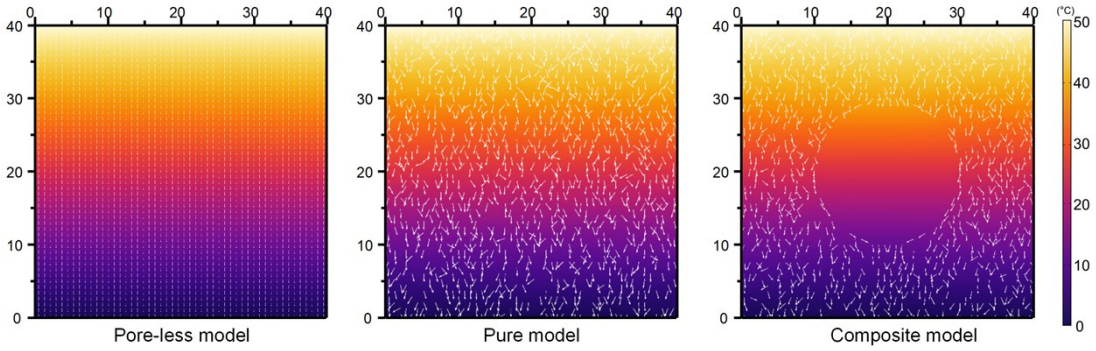

Figure S21. Heat flow directions in the thermal field.

Table S4. A comparison of mechanical properties between the F-3 film and other aerogels.

Materials	Structures	Preparation methods	Tensile strength (MPa)	References
Kevlar nanofiber aerogel (KNA)/phase-change materials (PCM)	Nanofibrous KNA film encapsulated by PCM	Freeze-drying	2.85	28
Ultrahigh molecular weight polyethylene (UHMW-PE)	Micro-macro hybrid porous structure	Thermal induced phase separation (TIPS) and particle leaching (PL)	2.48	29
Poly(vinylidenefluofide-co-hexafluoropropylene (P(VdF-HFP))/glass fibers (GF)	Composited aerogel structure	Freeze-drying	2.88	32
Polystyrene (PS)/polyamide6 (PA6)	PS microfiber film casted by PA6	Electrostatic spinning and solution casting	0.63	46
Hydroxyapatite Kevlar aerogel (HKA) /Kevlar -PCM gel (KPG)	Janus structure	Freeze-drying	1.20	47
Cellulose	Nano-pores aerogel structure	Twin screw extrusion	4.50	48
Meta-aramid/fluorinated hollow glass spheres aerogel films	Micro-nano porous structure	Sol-gel and hot-pressing	5.29	This work

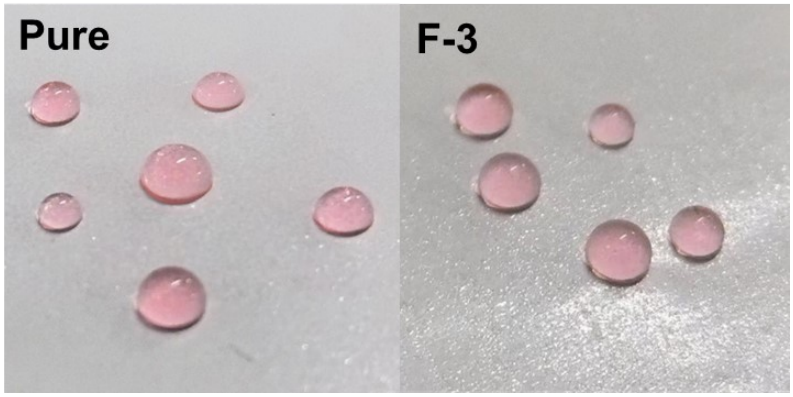

Figure S22. Optical pictures of water droplets placed on the surface of Pure and F-3 film.

References

1. Xiaokun Gu, Zheyong Fan, Hua Bao, *J. Appl. Phys.*, **2021**, 130, 210902.
2. Xinjian Liu, Zhonghao Rao, *Comp. Mater. Sci.*, **2020**, 172, 109298.
3. Md Masuduzzaman, BoHung Kim, *ACS Omega*, **2020**, 5, 26527.
4. Fatemeh Ahangaran, Amir H.Navarchian, *Adv. Colloid. Interface Sci.*, **2020**, 286, 102298.
5. Jiqiang Hu, Fei Li, Bing Wang, Hanqi Zhang, Chunming Ji, Shixun Wang, Zhengong Zhou, *Compos. B Eng.*, **2020**, 191, 107966.
6. Fui Kiew Liew, Sinin Hamdan, Md. Rezaur Rahman, Mohamad Rusop, Afrasyab Khan, *Polym. Compos.*, **2020**, 41, 4830.